Extraction and recovery of zinc, potassium, and sodium from blast furnace dust by ultrasonic-assisted ammonia leaching

JianTao Ju [1]*, YongWei Hu[1], Ning Luo[1], WenKe Guo[1], Qiang Bi[2]

1) School of Metallurgical Engineering, Xi'an University of Architecture and Technology, Xi'an 710055, China
2) School of Chemistry and Chemical Engineering, Xi'an University of Architecture and Technology, Xi'an 710055, China
*Corresponding author: JianTao Ju
E-mail: ju_jiantao@163.com

(Received 25 October 2025; Accepted 04 June 2026)

Abstract: To efficiently recover valuable elements (Zn, K, Na) from blast furnace dust (BFD) and address issues such as alkali metal enrichment and disrupted furnace operation caused by its direct reuse, ammonia leaching experiments were conducted in this study using an $NH_3 \cdot H_2O$–NH_4HCO_3 system combined with ultrasound and ammonium persulfate. Single-factor experiments were conducted to investigate the effects of factors (e.g., $[NH_3]_T$, solid-to-liquid ratio) on the leaching efficiencies of Zn, K, and Na under ultrasonic conditions. Under the conditions of $[NH_3]_T$ = 6 mol·L^{-1}, a solid-to-liquid ratio of 1:6, $[NH_3]/[NH_4^+]$ = 1:1, 40 °C, and 90 W ultrasound power, the leaching efficiencies of Zn, K, and Na reach 90.73%, 91.45%, and 91.56%, respectively. Based on this, the effect of ultrasound combined with 1 mol·L^{-1} ammonium persulfate on zinc leaching was further evaluated, and the Zn leaching efficiency was enhanced to 95.16%, while the leaching efficiencies of K and Na slightly increased to 92.35% and 92.50%, respectively. The enhanced Zn leaching is reasonably attributed to the synergistic effects of ultrasonic intensification and persulfate oxidation, in which ultrasound promotes particle fragmentation and mass transfer, while activated ammonium persulfate generates $SO_4^{\bullet-}$ radicals that facilitate the oxidation of refractory ZnS. Kinetic analysis indicated that Zn leaching was mainly controlled by the surface chemical reaction, and ultrasound reduced the apparent activation energy from 62.37 to 44.15 kJ·mol^{-1}. This synergistic leaching process, with high selectivity and low cost, provides theoretical and technical references for BFD resource recovery.

Keywords: blast furnace dust; zinc; ammoniacal leaching; ultrasonic; ammonium persulfate

1 Introduction

Blast furnace dust (BFD) is a fine particulate by-product captured by the bag filter system during blast furnace ironmaking. In addition to Fe and C, it is usually enriched in Zn, K, and Na. In China, the annual generation of BFD has exceeded 15 million tons, and its Zn content generally ranges from 1% to 10% [1,2]. Direct recirculation of BFD to the blast furnace can cause the accumulation of Zn and alkali metals, leading to

refractory accretion, tuyere blockage, unstable furnace operation, and shortened campaign life. Meanwhile, Zn, K, and Na in BFD are not only harmful circulating elements, but also valuable secondary resources. Among them, Zn is particularly important because ZnO has wide industrial applications and thus high recovery value [3]. In addition, the high Fe content of BFD implies that improper treatment would also waste valuable iron-bearing resources [4–6]. Therefore, the development of an efficient process for the selective removal and recovery of Zn, K, and Na from BFD is of clear industrial significance.

At present, BFD is mainly treated by pyrometallurgical and hydrometallurgical routes. Pyrometallurgical processes, such as rotary kilns and electric furnaces, can achieve relatively high metal recovery, but they are generally associated with high energy consumption, limited economic viability for low-grade zinc-bearing materials, and serious secondary dust pollution [7,8]. Hydrometallurgical processes have attracted more attention because of their lower energy demand, simpler operation, and lower cost. Acid leaching usually exhibits high leaching efficiency, but often suffers from poor selectivity toward Fe and severe equipment corrosion [9,10]. Alkaline leaching avoids Fe dissolution, but it often leaves a high Na content in the residue, which is unfavorable for direct recycling, while wastewater neutralization further increases the operating cost [11]. Therefore, a leaching system combining high selectivity with mild operating conditions is highly desirable.

Ammonia leaching is regarded as a promising method for zinc recovery from secondary resources because NH_3 can react with ZnO to form stable ammine complexes, while Fe in BFD is generally not leached under such conditions. Ammonia leaching systems include single-ammonia systems and ammonia–ammonium salt systems, the latter generally showing better performance [12]. Among them, ammonia–ammonium chloride provides relatively high ZnO leaching efficiency but introduces corrosive chloride ions [13], whereas ammonia–ammonium sulfate may weaken selectivity because a small amount of Fe can dissolve simultaneously [14]. By contrast, ammonia–ammonium carbonate and ammonia–ammonium bicarbonate systems combine good Zn leaching efficiency with high selectivity [15–17]. Compared with the carbonate system, the bicarbonate system operates under milder conditions, exhibits lower ammonia volatilization, simplifies solution purification, and benefits from the lower industrial cost of NH_4HCO_3. Therefore, it was selected in this study as the basic leaching medium. Moreover, because K and Na in BFD are commonly present as chlorides, the $NH_3{\cdot}H_2O$–NH_4HCO_3 system is also potentially suitable for their simultaneous leaching and recovery. However, the presence of a small amount of refractory ZnS in BFD still limits further improvement in zinc leaching efficiency.

Recent studies have shown that oxidants and ultrasonic intensification can significantly improve the leaching of refractory zinc-bearing phases. In ammoniacal systems, persulfate has been reported to oxidize ZnS and thereby enhance Zn extraction [18,19]. For example, Yang et al. reported that an ammonia–ammonium sulfate–ammonium persulfate system could selectively recover zinc from high-chloride zinc slag, achieving a Zn recovery rate of approximately 96% under optimized conditions; the improvement was mainly attributed to the oxidative dissolution of refractory ZnS

by ammonium persulfate [19]. Meanwhile, ultrasound can intensify solid–liquid reactions through cavitation-related effects and mass-transfer enhancement [20–23]. More importantly, ultrasound can also activate persulfate to generate strongly oxidizing sulfate radicals, which promote the breakdown of refractory sulfide phases while improving interfacial contact between the leachant and the solid particles [20,22]. These findings indicate that the combination of ultrasound and persulfate may provide an effective strategy to overcome the limiting effect of ZnS in the $NH_3·H_2O$–NH_4HCO_3 system.

Therefore, this study developed an ultrasound-assisted $NH_3·H_2O$–NH_4HCO_3 leaching system for the simultaneous recovery of Zn, K, and Na from BFD, optimized the main process parameters, and further evaluated the role of ammonium persulfate ($(NH_4)_2S_2O_8$) in enhancing Zn leaching. This process is simple, low-cost, and easy to regulate, and it provides theoretical support and technical guidance for the resource recovery and sustainable utilization of BFD.

2 Materials and methods

2.1 Experimental materials

The BFD sample is sourced from a steel company in Gansu, China. Its chemical composition is analyzed by ICP-MS, with results summarized in Table 1. As presented in Table 1, the main components of BFD are Fe, C, and Zn. Zn, K, and Na contents are 5.90 wt%, 4.86 wt%, and 0.39 wt%, respectively. Fig. 1 reveals that Fe mainly exists as hematite, with a minor presence of magnetite. Zn is primarily present as zinc oxide (ZnO) and zinc ferrite ($ZnFe_2O_4$), with a small amount as zinc sulfide (ZnS). Potassium mainly exists in the form of potassium chloride (KCl). Quantitative phase analysis was conducted by Rietveld refinement of the XRD pattern shown in Fig. 1. The results revealed that the sample was mainly composed of Fe_2O_3 (66.6%), Fe_3O_4 (5.4%), KCl (7.4%), ZnS (3.4%), $ZnFe_2O_4$ (11.1%), and ZnO (6.2%). The Rietveld refinement indicates that ZnS accounts for 3.4 wt% of the BFD sample, confirming the presence of a non-negligible refractory zinc sulfide phase that justifies the introduction of persulfate oxidation.

The reagents required for this experiment were as follows: ammonia solution ($NH_3·H_2O$, 25–28 wt%, AR grade, Tianjin Fuyu Fine Chemical Co., Ltd.), ammonium bicarbonate (NH_4HCO_3, 21.0–22.0 wt% as NH_3, AR grade, Tianjin Damao Chemical Reagent Factory).

Table 1. Chemical Composition of BFD /(wt.%)

Element	Fe	Si	Zn	K	Na	S	C
Wt%	50.16	3.28	5.90	4.86	0.39	0.60	20.90

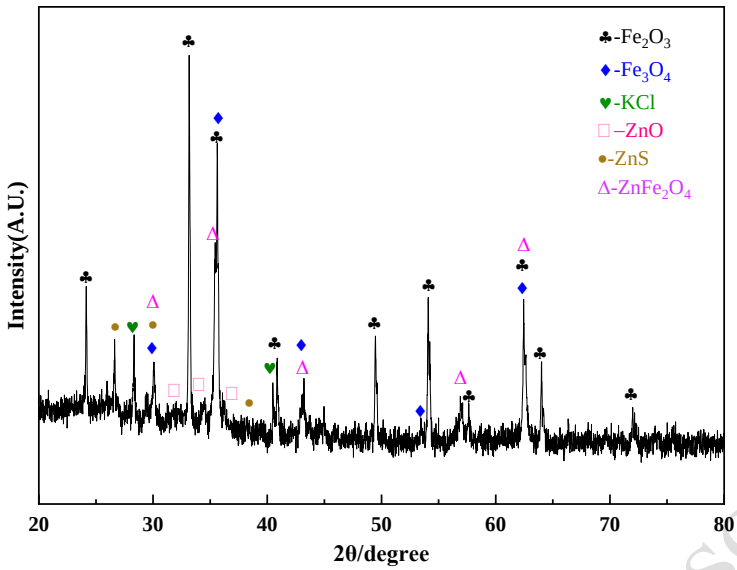

Fig. 1. XRD pattern of BFD

2.2 Experimental procedure

Prior to the experiment, the BFD raw material was dried in an oven at 80 °C for 24 h. The dried sample was ground, sieved through a 200-mesh standard sieve, and stored in a desiccator at room temperature for subsequent use.

Ammonia leaching solutions of the desired concentrations were prepared according to the calculated compositions and then mixed with the pretreated BFD samples. Ultrasound-assisted ammonia leaching experiments were carried out in a digitally controlled ultrasonic cleaner (KQ3200DE, Kunshan Ultrasonic Instrument Co., Ltd.) operated at a fixed frequency of 40 kHz, whereas conventional ammonia leaching experiments were performed in a thermostatic water bath shaker (HH-6B, Guohua Instrument Manufacturing Co., Ltd.). After leaching, the slurry was vacuum-filtered using a rotary vane vacuum pump (2XZ-1, Beijing Yong Guang Ming Medical Instrument Co., Ltd.) to separate the filtrate from the residue. The residue was dried at 80 °C for 6 h and stored for subsequent analyses.

(1) Determination of Zn, K, Na and Fe elements

One milliliter of filtrate was diluted to a certain factor and the concentrations of Zn, K, Na and Fe in the filtrate were measured using a flame atomic absorption spectrophotometer (AA-6800, Shimadzu Hong Kong Instruments Ltd.). The leaching rate was calculated according to Eq. (1) to optimize experimental parameters. The metal ion leaching rate was calculated as follows:

$$\omega = \frac{C_x \times V}{W_x} \times 100\% \quad (1)$$

Where ωx is the leaching rate of the metal element; Cx is the concentration of the metal element in the filtrate ($mg \cdot L^{-1}$); V is the volume of the leaching solution (mL); and Wx is the content of the element in the BFD.

(2) Phase analysis

The phase composition of the leaching residue is analyzed using an X-ray diffractometer

(XRD, Bruker D8 ADVANCE, China) under the following conditions: 40 kV, 40 mA,

2θ scan range of 20°–90°, and a scan rate of 8.75°/min.

(3) Morphological analysis

The microstructure and chemical composition of the samples are examined using a scanning electron microscope equipped with energy-dispersive spectroscopy (SEM-EDS, GeminiSEM 500, Germany). SEM was employed to observe the morphological variations under different experimental conditions, and EDS was used only for the semi-quantitative comparison of local main elemental compositions before and after leaching, rather than for the determination of overall absolute compositions.

2.3 Experimental principle

In the Zn–NH_3·H_2O–NH_4HCO_3 system, ZnO in BFD complexes with free ammonia to form zinc–ammonia complexes (Eq. 2). As $[NH_3]_T$ increases, both the pH and the concentration of free ammonia increase, thereby promoting zinc–ammonia complexation. When pH<8, Zn^{2+} predominates and complexation is weak. At pH 8–11, $[Zn(NH_3)_4]^{2+}$ becomes the dominant species, which is favorable for zinc leaching. Low $[NH_3]_T$ keeps the pH relatively low, limits complex formation, and reduces the leaching efficiency. Conversely, excessive alkalinity promotes the reaction of Zn^{2+} with CO_3^{2-} and HCO_3^- to form $ZnCO_3$ or basic zinc carbonate (Eqs.3–4) and causes $[Zn(NH_3)_4]^{2+}$ to react with OH^- to form $Zn(OH)_2$, which can redissolve at even higher pH (Eqs.5–7), thereby increasing reagent consumption unnecessarily. Therefore, excessive additions of ammonia and ammonium bicarbonate should be avoided.

$$ZnO + nNH_3 + H_2O \longrightarrow [Zn(NH_3)_n]^{2+} + 2OH^-$$

$$Zn^{2+} + CO_3^{2-} \rightarrow ZnCO_3$$

$$Zn^{2+} + HCO_3^- \rightarrow Zn(HCO_3)^+$$

$$Zn(NH_3)_4^{2+} + 2OH^- \rightarrow Zn(OH)_2 + 4NH_3$$

$$Zn(OH)_2 + 2OH^- \rightarrow Zn(OH)_4^{2-}$$

$$Zn(OH)_4^{2-} + 2OH^- \rightarrow Zn(OH)_6^{2-}$$

3 Results and discussion

3.1 Single-factor experiments

The leaching efficiencies of Zn, K, and Na from BFD in the ultrasound-assisted NH_3·H_2O–NH_4HCO_3 system were investigated by single-factor experiments. With other conditions kept constant, the effects of $[NH_3]_T$, solid-to-liquid ratio, ammonia-to-ammonium ratio ($[NH_3]/[NH_4^+]$), temperature, and ultrasonic power on leaching efficiency were examined. Subsequently, the promoting effect of $(NH_4)_2S_2O_8$ concentration on Zn leaching was evaluated. Leaching efficiency was calculated using Eq. (1), and each experiment was repeated three times; the average value was used to minimize random error.

The selected parameter ranges were chosen to cover the practically relevant operating window of the NH_3·H_2O–NH_4HCO_3 leaching system while avoiding excessively extreme conditions. Specifically, $[NH_3]_T$ values of 4-7 mol·L^{-1} were used to span insufficient and excess free-ammonia conditions; solid-to-liquid ratios of 1:3–1:7 were selected to reflect the trade-off between mass transfer and reagent consumption; $[NH_3]/[NH_4^+]$ ratios from 3:1 to 1:3 were used to vary the balance between complexation capacity and buffering; temperatures of 30-60 °C were adopted to evaluate kinetic enhancement before severe ammonia volatilization or NH_4HCO_3

decomposition; ultrasonic powers of 60-150 W were examined to assess cavitation intensification while avoiding excessive bubble coalescence; and $(NH_4)_2S_2O_8$ concentrations of 0.5–2.0 mol·L^{-1} were investigated to determine the oxidant dosage required for ZnS oxidation without excessive non-productive oxidant consumption. On this basis, the influence of each factor on Zn, K, and Na leaching was analyzed systematically, and the optimum conditions were identified from the combined response trends.

3.1.1 Effect of $[NH_3]_T$

The effect of different total ammonia concentrations ($[NH_3]_T$=4, 5, 6, and 7 mol·L^{-1}) on the leaching behavior of Zn, K, and Na was investigated. Fig. 2(a) presents the influence of $[NH_3]_T$ on Zn leaching efficiency at different leaching times. As the leaching time increased, the Zn leaching efficiency first rose rapidly and then approached a plateau. At $[NH_3]_T$=4 mol·L^{-1} and 120 min, the maximum Zn leaching efficiency was 79.12%. With further increases in $[NH_3]_T$, the Zn leaching efficiency initially increased and then stabilized, reaching 85.38% at $[NH_3]_T$=6 mol·L^{-1} and 100 min. This is because, at $[NH_3]_T$=4–6 mol·L^{-1}, the increase in ammonia concentration promotes Zn–ammonia complexation, thereby enhancing Zn leaching. However, when $[NH_3]_T$>6 mol·L^{-1}, ammonia saturation and volatilization limit the improvement in leaching efficiency [16].

As shown in Fig. 2(b), the leaching efficiencies of K and Na slightly increased with increasing $[NH_3]_T$, peaking at 89.41% (7 mol·L^{-1}) and 90.70% (6 mol·L^{-1}), respectively. On the one hand, ultrasound can fragment the mineral particles, thereby directly releasing soluble potassium and sodium salts from the particles. On the other hand, salt solubility is higher under alkaline conditions; increasing the total ammonia concentration raises the solution pH, and OH^- reacts with aluminosilicate minerals, thereby promoting the release of K^+ and Na^+ [24].

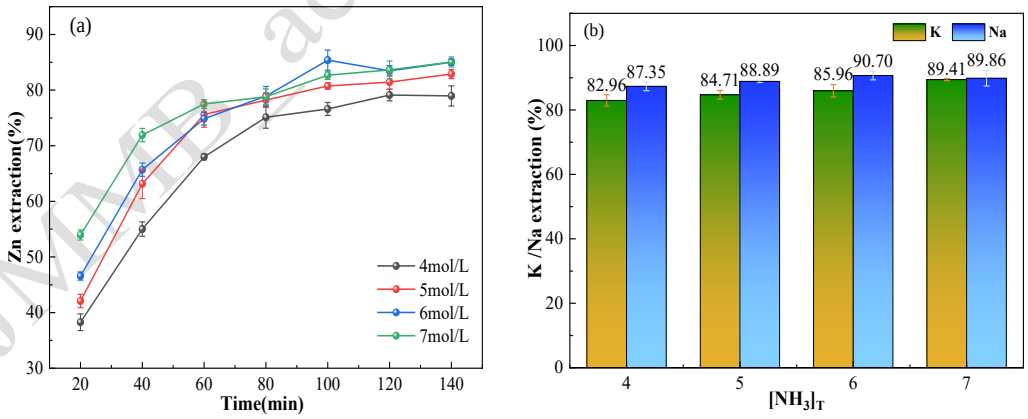

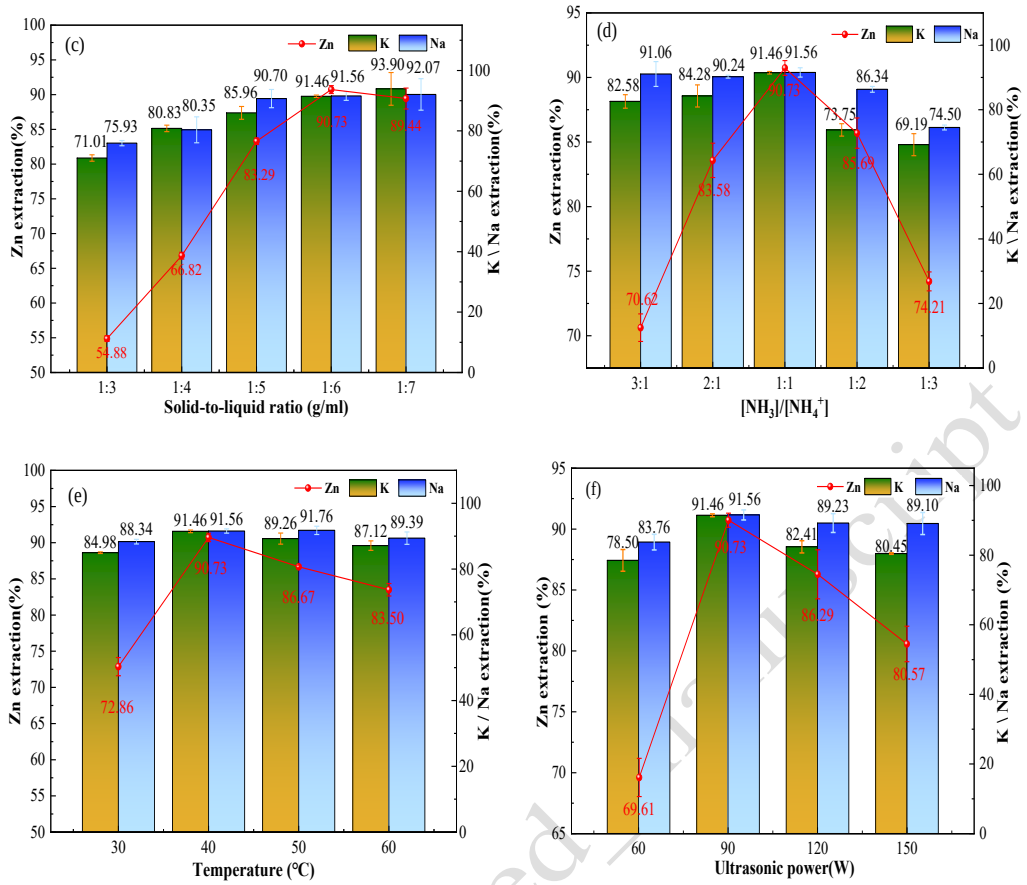

Fig. 2. (a) Zn leaching rate vs. time at different $[NH_3]_T$; (b) K and Na leaching rates at different $[NH_3]_T$; (c) effect of solid-to-liquid ratio; (d) effect of $[NH_3]/[NH_4^+]$ ratio; (e) effect of temperature; and (f) effect of ultrasonic power. (Some error bars are smaller than the symbols)

3.1.2 Effect of solid-to-liquid ratio

With $[NH_3]_T$ fixed at 6 $mol \cdot L^{-1}$ and the other conditions unchanged, the effect of different solid-to-liquid ratios (1:3, 1:4, 1:5, 1:6, and 1:7) on the leaching efficiencies of Zn, K, and Na was investigated. As shown in Fig. 2(c), when the solid-to-liquid ratio decreased from 1:3 to 1:5, the Zn leaching efficiency increased. When the ratio exceeded 1:5, the leaching rate gradually stabilized, and at a ratio of 1:6 the Zn leaching efficiency reached a maximum of 90.73%. At a ratio of 1:3, the low Zn leaching efficiency is attributed to the increased mass-transfer resistance caused by the high solid content, which reduced the diffusion rate of Zn^{2+} and limited the reaction rate. As the ratio decreased, the slurry concentration and viscosity were reduced, thereby diminishing mass-transfer resistance and promoting the reaction [25]. However, when the ratio was further reduced from 1:6 to 1:7, the Zn leaching efficiency changed only slightly because the Zn–ammonia complexation equilibrium had been essentially reached. Further dilution therefore had little effect on Zn leaching while increasing reagent consumption and equipment load [14].

Similarly, as the solid-to-liquid ratio decreases, the reduced mass transfer resistance facilitates the leaching of K and Na. Their leaching efficiencies first increase rapidly and then stabilize, reaching maximum values of 93.90% and 92.07%, respectively, at a ratio of 1:7. Considering both leaching efficiency and economic

feasibility, a solid-to-liquid ratio of 1:6 is determined to be optimal.

3.1.3 Effect of $[NH_3]/[NH_4^+]$ ratio

Under the conditions of $[NH_3]_T$=6 mol·L^{-1}, a solid-to-liquid ratio of 1:6, and the other parameters held constant, the effect of different $[NH_3]/[NH_4^+]$ ratios (3:1, 2:1, 1:1, 1:2, and 1:3) on Zn leaching was investigated. As shown in Fig. 2(d), when $[NH_3]/[NH_4^+]$ = 3:1, the Zn leaching rate reached a minimum of 70.62%. As the $[NH_3]/[NH_4^+]$ ratio decreased, the Zn leaching efficiency first increased and reached a maximum of 90.73% at $[NH_3]/[NH_4^+]$=1:1. Thereafter, it began to decrease, and the Zn leaching efficiency was only 74.21% when $[NH_3]/[NH_4^+]$=1:3.

The reason for this phenomenon is as follows. On the one hand, metal leaching essentially involves the formation of soluble complexes between target ions and NH_3. When $[NH_3]/[NH_4^+]$=1:1, the free NH_3 concentration and complex stability reach a favorable balance. When $[NH_3]/[NH_4^+]$<1, excess NH_4^+ results in insufficient free NH_3 in solution, which prevents full coordination with metal ions; for example, Zn^{2+} cannot readily form stable $[Zn(NH_3)_4]^{2+}$, resulting in low leaching efficiency. When $[NH_3]/[NH_4^+]$>1, excess NH_3 enhances coordination capacity but also intensifies NH_3 volatilization, especially at elevated temperature, thereby reducing the concentration of effective complexing species in the system. In addition, excessive free ammonia may reduce selectivity by promoting the co-leaching of impurity ions [15,26]. On the other hand, as the $[NH_3]/[NH_4^+]$ ratio approaches 1:1, the content of soluble NH_3 increases. Since dissolved gases may act as nucleation sites for ultrasonic cavitation, a higher NH3 content may be more favorable for cavitation-related ultrasonic intensification, which is consistent with previous reports [27].

Similarly, as $[NH_3]/[NH_4^+]$ decreases, the lower pH suppresses the release of soluble K^+ and Na^+ from minerals and causes their leaching efficiencies to decline. Therefore, $[NH_3]/[NH_4^+]$=1:1 was selected as the optimal ammonia-to-ammonium ratio.

3.1.4 Effect of leaching temperature

Under controlled conditions of $[NH_3]_T$ = 6 mol·L^{-1}, a solid-to-liquid ratio of 1:6, $[NH_3]/[NH_4^+]$=1:1, and the other parameters kept constant, the effect of leaching temperature (30, 40, 50, and 60 °C) on the leaching rates of Zn, K, and Na was investigated. As shown in Fig. 2(e), at 30 °C the Zn leaching rate reached only 72.86%. When the temperature increased to 40 °C, the Zn leaching rate peaked at 90.73%. However, at 50 °C, the Zn leaching rate decreased to 86.67%. Similar to Zn, the leaching rates of K and Na first increased slightly and then decreased slightly, reaching maximum values of 89.26% and 91.76%, respectively.

The initial increase in Zn leaching between 30 and 40°C is attributed to enhanced reactant activity and accelerated leaching kinetics, together with reduced slurry viscosity and improved molecular diffusion, which facilitate the complexation of ZnO with ammonia ligands. When the temperature exceeded 40°C, the volatilization of NH_3 and the decomposition of NH_4HCO_3 increased, reducing the ammonia available for Zn coordination and causing a decline in Zn leaching. The slight decrease in K and Na leaching at higher temperatures is likely due to increased NH_3 volatilization and the associated decrease in solution pH, which suppress the alkaline release of entrapped K^+ and Na^+. Considering these factors, 40°C was identified as the optimal leaching

temperature.

3.1.5 Effect of ultrasonic power on leaching efficiency

Under controlled conditions of $[NH_3]_T$=6 mol·L^{-1}, a solid-to-liquid ratio of 1:6, $[NH_3]/[NH_4^+]$=1:1, 40 °C, and the other parameters kept constant, the effect of ultrasonic power (60, 90, 120, and 150 W) on the leaching rates of Zn, K, and Na was investigated. As shown in Fig. 2(f), when the ultrasonic power was 60 W, the Zn leaching rate reached 69.61%. With an increase in ultrasonic power, the leaching efficiency of Zn first increased and then decreased, reaching a maximum value of 90.73% at 90 W. In contrast, the leaching efficiencies of potassium and sodium both reached their maximum values at an ultrasonic power of 90 W and then decreased.

As the ultrasonic power increased from 60 W to 90 W, the leaching efficiency of Zn increased markedly. This enhancement is generally attributed to ultrasonic cavitation and the associated intensification of particle collision and mass transfer [28]. The reduction in residue particle size and the fragmented morphology observed after leaching are consistent with such an intensification effect, although cavitation was not directly measured. In addition, cavitation-related microstreaming and surface cleaning may improve the contact between the leaching solution and Zn-bearing phases, thereby shortening the reaction time [29]. When the ultrasonic power became excessively high, the effective leaching enhancement of Zn, K, and Na was weakened, which may be associated with changes in bubble dynamics and a decrease in cavitation efficiency. Considering these factors, 90 W was determined to be the optimal ultrasonic power.

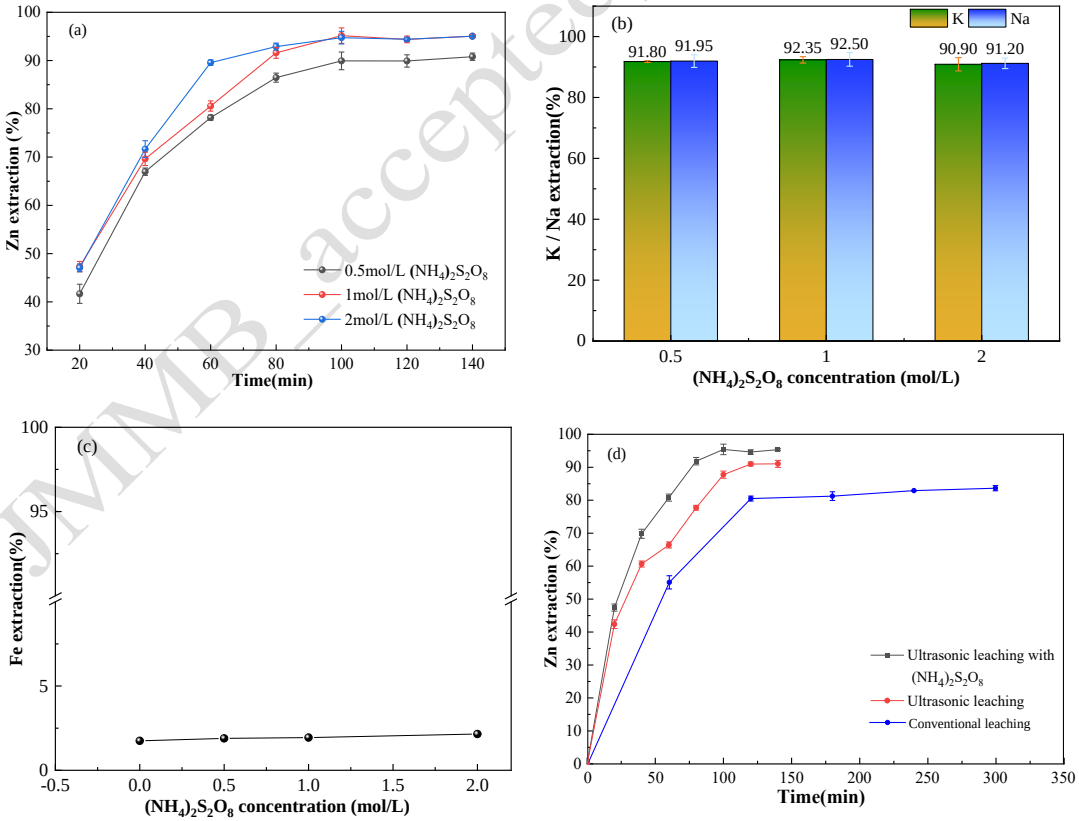

Fig. 3. (a) Zn leaching rate vs. time at different $(NH_4)_2S_2O_8$ concentrations; (b) Leaching rates of K and Na at different $(NH_4)_2S_2O_8$ concentrations; (c) Leaching rates of Fe at different $(NH_4)_2S_2O_8$ concentrations. (d) Comparison of Zn leaching rates among ultrasound leaching, ultrasound with

$(NH_4)_2S_2O_8$, and conventional leaching.

3.1.6 Effect of $(NH_4)_2S_2O_8$ concentration on metal leaching efficiency

Under the optimal conditions ($[NH_3]_T$= 6 mol·L^{-1}, solid-to-liquid ratio = 1:6, $[NH_3]/[NH_4^+]$= 1:1, 40 °C, and ultrasonic power = 90 W), the ultrasound-assisted $NH_3·H_2O$–NH_4HCO_3 system significantly improved Zn leaching from BFD, yielding leaching efficiencies above 90%. However, XRD analysis of the raw material revealed the presence of a small amount of chemically stable ZnS in BFD, which is difficult to leach using conventional ammonia leaching alone. Because of its strong oxidizing properties, $(NH_4)_2S_2O_8$ can oxidatively leach ZnS in alkaline solution under activation conditions. To investigate the oxidative leaching effect of $(NH_4)_2S_2O_8$ on ZnS and further enhance Zn recovery, $(NH_4)_2S_2O_8$ was added to the ultrasound-assisted ammonia leaching system while the other parameters were kept at their optimum values. The effects of varying $(NH_4)_2S_2O_8$ concentrations (0.5, 1.0, and 2.0 mol·L^{-1}) on the leaching efficiencies of Zn, K, Na, and Fe were evaluated, and the results are shown in Fig. 3. For Fe leaching, an additional control experiment without $(NH_4)_2S_2O_8$ addition was included under the optimized ultrasound-assisted ammonia leaching conditions.

As shown in Fig. 3(a), the Zn leaching rate increased as the $(NH_4)_2S_2O_8$ concentration rose from 0.5 to 1.0 mol·L^{-1} and reached 95.16% at 1.0 mol·L^{-1} after 100 min. This behavior may be attributed to two factors. First, after dissolution, $S_2O_8^{2-}$ is activated by ultrasonic irradiation to generate sulfate radicals ($SO_4^{\bullet-}$) (Eqs. 8–9). Because $SO_4^{\bullet-}$ has strong oxidizing ability, it can react with ZnS in the alkaline slurry and release Zn into solution [30,31] (Eqs. 10–11). Second, $SO_4^{\bullet-}$ reacts with dissolved NH_3 to generate small amounts of N_2 and H^+; the generated H^+ then reacts with HCO_3^-, and the buffering capacity of HCO_3^- prevents a pronounced pH decrease, while producing fine CO_2 bubbles [32] (Eqs. 12–13). The rising fine N_2 and CO_2 bubbles create turbulence, enhance solid–liquid mixing, reduce local concentration gradients, and promote contact between the ore particles and the leaching agent, thereby accelerating the transfer of metal ions from the ore surface to solution. A schematic illustration of this process is shown in Fig. 4. Accordingly, adding an appropriate amount of $(NH_4)_2S_2O_8$ improves Zn leaching efficiency. However, when the $(NH_4)_2S_2O_8$ concentration reached 2.0 mol·L^{-1}, excessive ultrasonically activated $SO_4^{\bullet-}$ consumed large amounts of NH_3, which decreased the Zn leaching efficiency.

As shown in Fig. 3(b), the leaching efficiencies of K and Na changed only slightly with the addition of $(NH_4)_2S_2O_8$. When the $(NH_4)_2S_2O_8$ concentration increased from 0.5 to 1.0 mol·L^{-1}, the K and Na leaching efficiencies increased from 91.80% and 91.95% to 92.35% and 92.50%, respectively. However, when the concentration further increased to 2.0 mol·L^{-1}, the leaching efficiencies decreased to 90.90% and 91.20%, respectively. This indicates that $(NH_4)_2S_2O_8$ has no direct oxidative leaching effect on K- and Na-bearing phases. The slight improvement at an appropriate dosage is mainly related to enhanced mixing, particle fragmentation, and mass transfer caused by ultrasonic activation and bubble generation. In contrast, excessive $(NH_4)_2S_2O_8$ may consume dissolved NH_3 and weaken the alkaline environment, thereby slightly suppressing the release of K^+ and Na^+.

As shown in Fig. 3(c), under the optimized ultrasound-assisted ammonia leaching conditions without $(NH_4)_2S_2O_8$ addition, the Fe leaching efficiency was only 1.75%. After adding $(NH_4)_2S_2O_8$, the Fe leaching efficiency increased slightly from 1.89% to 2.15% with increasing $(NH_4)_2S_2O_8$ concentration, but remained below 3% throughout the investigated range. This negligible Fe dissolution indicates that the $NH_3{\cdot}H_2O$–NH_4HCO_3 system maintained good selectivity even after the addition of $(NH_4)_2S_2O_8$. Since Fe in BFD mainly exists as Fe_2O_3 and Fe_3O_4, these iron-bearing phases are difficult to dissolve in the weakly alkaline ammoniacal system. Therefore, Fe was mainly retained in the leaching residue, whereas Zn, K, and Na were selectively leached into solution. Considering the leaching efficiencies of Zn, K, Na, and Fe, 1.0 $mol{\cdot}L^{-1}$ was identified as the optimal $(NH_4)_2S_2O_8$ concentration.

$$(NH_4)_2S_2O_8 \longrightarrow S_2O_8^{2-} + 2NH_4^+$$
$$S_2O_8^{2-} \xrightarrow{Ultrasonic} 2SO_4^{\cdot-}$$
$$ZnS + 4NH_3 + 2SO_4^{\cdot-} \longrightarrow [Zn(NH_3)_4]^{2+} + S\downarrow + 2SO_4^{2-}$$
$$ZnS + 12NH_3 + 8SO_4^{\cdot-} + 4H_2O \longrightarrow [Zn(NH_3)_4]^{2+} + 9SO_4^{2-} + 8NH_4^+ \quad (11)$$
$$2NH_3 + 6SO_4^{\cdot-} \longrightarrow N_2\uparrow + 6SO_4^{2-} + 6H^+$$
$$H^+ + HCO_3^- \longrightarrow H_2O + CO_2\uparrow$$

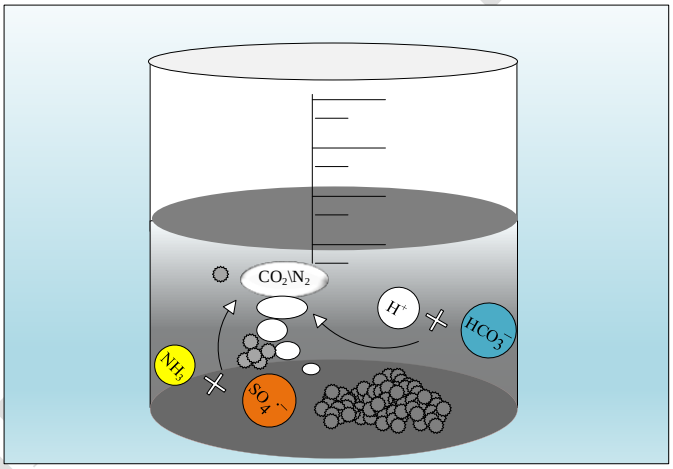

Fig. 4. Schematic illustration of bubble generation reactions after the addition of ammonium persulfate.

3.1.7 Comparative experiments

To clarify the effects of ultrasound and $(NH_4)_2S_2O_8$ on Zn leaching efficiency, a traditional leaching experiment (control group) was conducted at 300 rpm (preliminary tests confirmed this as the optimal stirring speed for conventional ammonia leaching). Other parameters were maintained at optimal values: $[NH_3]_T$= 6 $mol{\cdot}L^{-1}$, solid-to-liquid ratio= 1:6, $[NH_3]/[NH_4^+]$= 1:1, and 40 °C. Its results were compared with those of the optimal ultrasound-assisted ammonia leaching group and ultrasound-activated $(NH_4)_2S_2O_8$ ammonia leaching group (Fig. 3(d)). As shown, the control group exhibited an overall slower reaction rate: Zn leaching rate reached 80.50% at 120 min, then plateaued to a maximum of 83.65% at 300 min. In contrast, both ultrasound-containing groups showed significantly higher Zn leaching efficiencies than the control, with the

ultrasound-activated $(NH_4)_2S_2O_8$ group performing best. This group achieved the highest leaching rate (95.16%) at 100 min—7.77% higher than the ultrasound-assisted group, which peaked at 90.73% at 120 min. Both ultrasound groups essentially completed leaching by these times. In summary, ultrasound and $(NH_4)_2S_2O_8$ significantly enhance Zn leaching from BFD. Under optimal conditions, the ultrasound-activated $(NH_4)_2S_2O_8$ group exhibits a Zn leaching rate 4.43% and 11.51% higher than the ultrasound-assisted and control groups, respectively, while reducing leaching time by 16.67% and 66.67%, respectively.

3.2 Kinetic analysis

Considering that the Zn leaching efficiency decreased when the temperature was further increased above the optimal temperature of 40 °C, higher-temperature data were not used for kinetic fitting to avoid deviations caused by ammonia volatilization and NH_4HCO_3 decomposition rather than the intrinsic leaching reaction. To further clarify the leaching behavior and rate-controlling step of Zn dissolution, kinetic experiments were carried out at 20, 30, and 40 °C under conventional ammonia leaching and ultrasonic ammonia leaching conditions. As shown in Fig. 5, the Zn leaching efficiency increased with increasing leaching time and temperature in both systems. Compared with conventional leaching, ultrasonic leaching exhibited a higher Zn leaching efficiency at the same temperature and reaction time, indicating that ultrasound effectively promoted the dissolution of Zn-bearing phases.

To identify the rate-controlling step, the Zn leaching process was analyzed using the shrinking core model, as expressed in Eqs. (14)-(16). Eq. (14) represents the surface chemical reaction control model, Eq. (15) represents the internal diffusion control model, and Eq. (16) represents the mixed control model:

$$K_1 \cdot t = 1 - (1-\alpha)^{\frac{1}{3}} \tag{14}$$

$$K_2 \cdot t = 1 - \frac{2}{3}\alpha - (1-\alpha)^{\frac{2}{3}} \tag{15}$$

$$K_3 \cdot t = \frac{1}{3} ln(1-\alpha) - [1-(1-\alpha)]^{-\frac{1}{3}} \tag{16}$$

In Eqs. (14)-(16), α represents the Zn leaching fraction, k is the apparent rate constant, and t is the leaching time.

The fitting results are shown in Fig. 6. For both conventional and ultrasonic ammonia leaching, the apparent rate constants increased with increasing temperature, indicating that elevated temperature accelerated Zn dissolution. Among the three kinetic models, the surface chemical reaction control model showed good linearity and provided a physically reasonable description of the Zn leaching process over the investigated temperature range. Therefore, the rate constants derived from this model were used for the subsequent Arrhenius analysis.

The relationship between the apparent rate constant and temperature was further fitted using the Arrhenius equation:

$$K_0 = A \cdot \exp\left(-\frac{E_a}{RT}\right) \tag{17}$$

In Eqs. (17), E_a represents the apparent activation energy, R is the gas constant, and T is the absolute temperature.

As shown in Fig. 7, the Arrhenius plots exhibited good linearity for both conventional and ultrasonic ammonia leaching. The apparent activation energies calculated from the slopes were 62.37 kJ·mol^{-1} and 44.15 kJ·mol^{-1} for conventional leaching and ultrasonic leaching, respectively. The lower activation energy under ultrasonic conditions indicates that ultrasound reduced the energy barrier of Zn dissolution by enhancing cavitation, particle fragmentation, interfacial renewal, and mass transfer. Since both apparent activation energies were higher than 40 kJ·mol^{-1}, Zn leaching in the $NH_3·H_2O$–NH_4HCO_3 system was mainly controlled by the surface chemical reaction [33]. However, diffusion-related processes may also contribute to the overall leaching behavior, especially at the later stage of leaching.

Overall, ultrasonic intensification improved the Zn leaching rate and reduced the apparent activation energy, but it did not fundamentally change the dominant rate-controlling step. The leaching process was mainly governed by surface chemical reaction control, while ultrasound enhanced the accessibility of reactive Zn-bearing phases and promoted the transfer of dissolved Zn species from the solid surface into the solution.

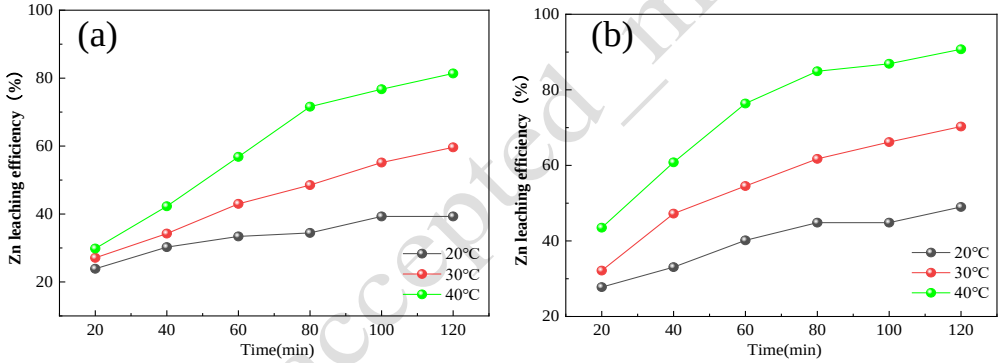

Fig. 5. Leaching kinetics experiments:(a) conventional leaching experiment; (b) ultrasonic leaching experiment

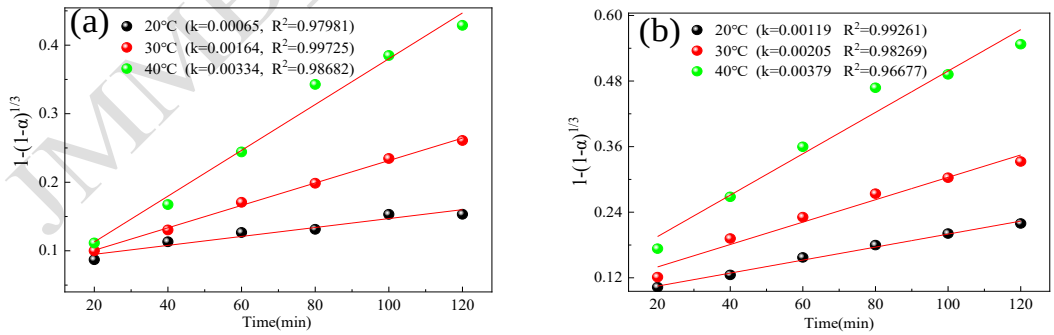

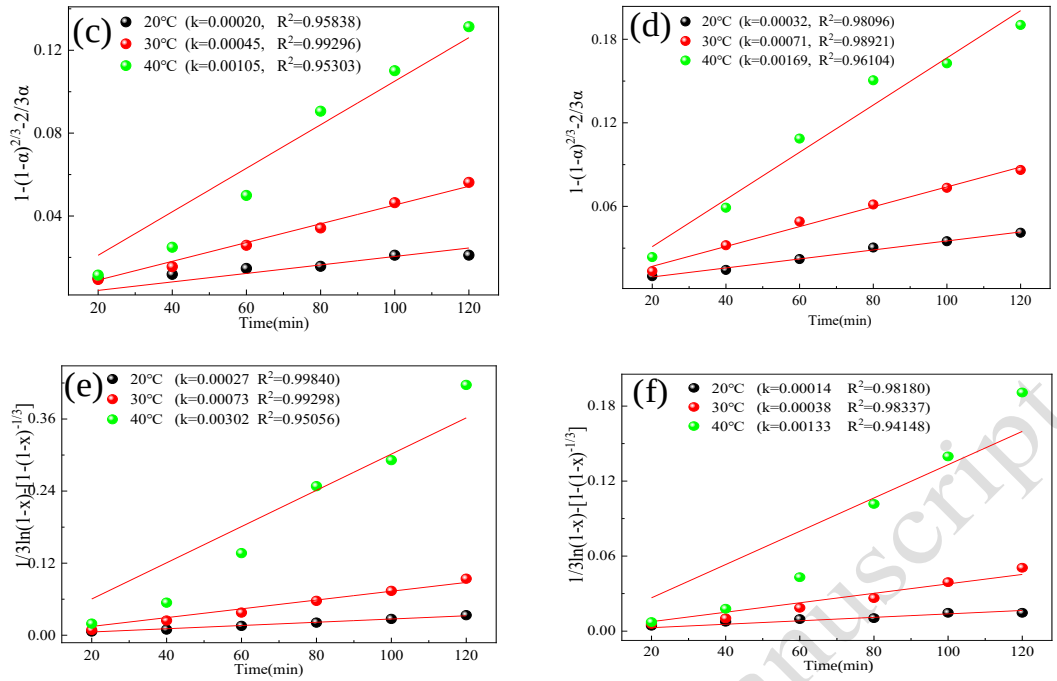

Fig. 6. Fitting results of the shrinking core model: (a), (c), and (e) represent the surface chemical reaction control, internal diffusion control, and mixed control models under conventional ammonia leaching, respectively; (b), (d), and (f) represent the corresponding models under ultrasonic ammonia leaching, respectively.

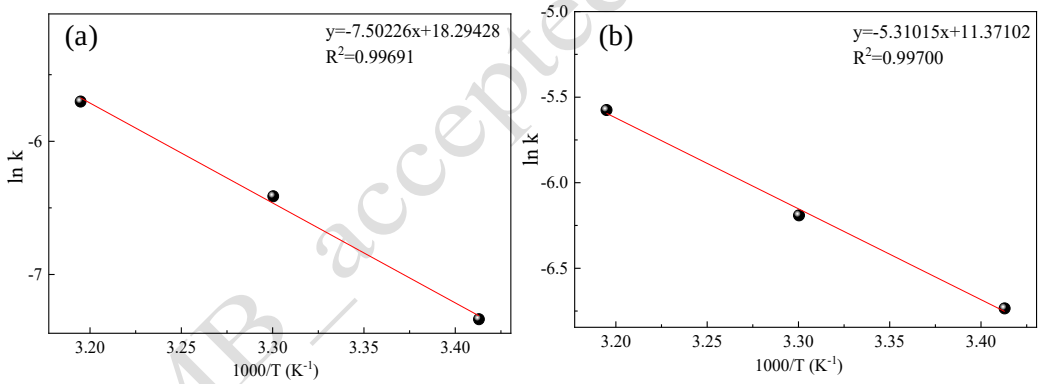

Fig. 7. Arrhenius plots for surface chemical reaction control: (a) Conventional leaching; (b) Ultrasonic leaching

3.3 Analysis of leaching residues

3.3.1 XRD analysis

Fig. 8 shows the XRD patterns of the BFD raw material and the residues obtained after conventional ammonia leaching, ultrasound-assisted ammonia leaching, and ultrasound-activated $(NH_4)_2S_2O_8$ ammonia leaching. In the residues from conventional and ultrasound-assisted leaching, the peaks of KCl and ZnO are significantly reduced or disappear, whereas the peaks of ZnS, Fe_2O_3, and Fe_3O_4 remain essentially unchanged. This indicates that KCl, owing to its high water solubility, is efficiently leached, whereas ZnO is selectively dissolved through coordination with ammonia ligands; in both cases, iron-bearing phases remain largely unaffected. However, because ZnS is chemically stable, conventional ammonia leaching cannot remove it effectively. In contrast, the ultrasound-activated $(NH_4)_2S_2O_8$ system markedly reduces both the ZnO

and ZnS peaks, confirming the efficient leaching of these phases. This result is reasonably attributed to the strongly oxidizing sulfate radicals ($SO_4^{\bullet-}$) generated from $(NH_4)_2S_2O_8$ under ultrasonic activation, which are likely responsible for promoting the oxidation and breakdown of ZnS.

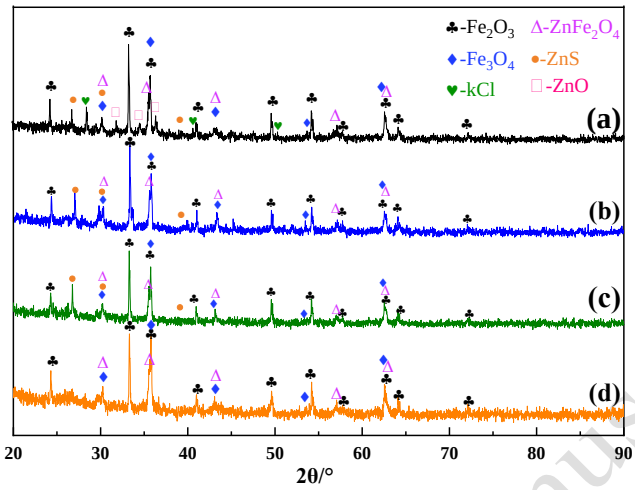

Fig. 8. XRD patterns of BFD and leaching residues: (a) BFD raw material; (b) residue from conventional ammonia leaching; (c) residue from ultrasound-assisted ammonia leaching; (d) residue from ultrasound-activated $(NH_4)_2S_2O_8$ ammonia leaching.

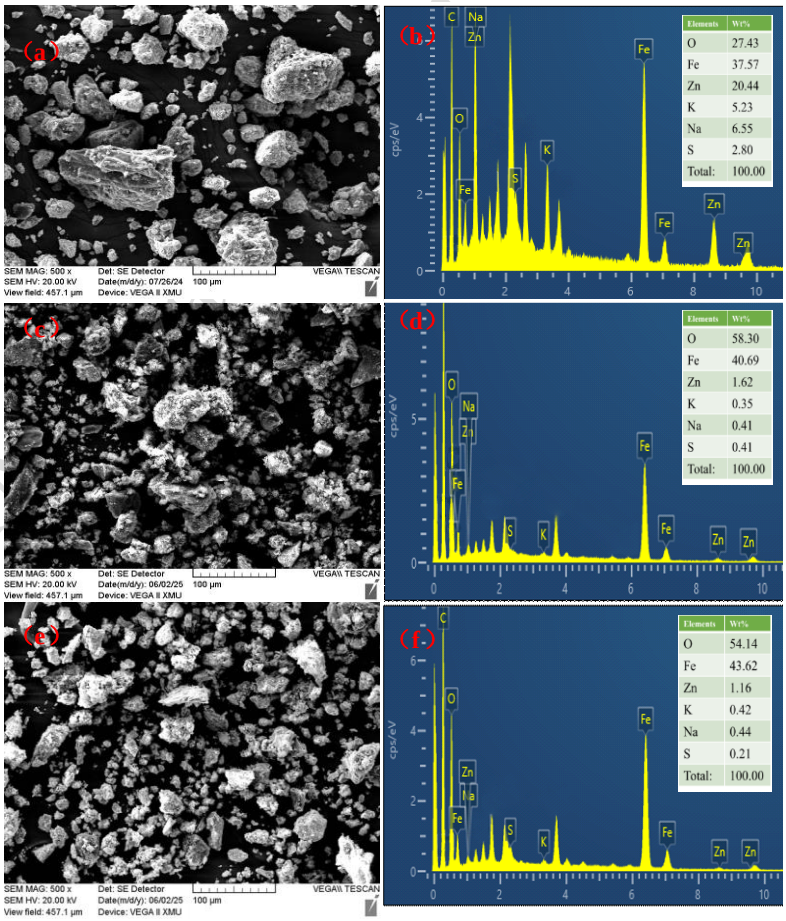

Fig. 9. SEM images and corresponding EDS spectra of the raw material and leaching residues: (a, b) BFD raw material; (c, d) residue from ultrasound-assisted ammonia leaching under

optimal conditions; (e, f) residue from ultrasound-activated $(NH_4)_2S_2O_8$ ammonia leaching under optimal conditions. The EDS spectra are presented for semi-quantitative local compositional comparison only.

Table 2. Particle-size statistics of the raw material and leaching residues (μm)

Sample	Minimum particle size	Maximum particle size	Average particle size
BFD raw material	3.49	147.53	23.26
Ultrasound-assisted residue	2.98	75.84	18.30
Ultrasound-activated $(NH_4)_2S_2O_8$ residue	3.04	69.03	16.35

3.3.2 SEM and EDS analysis

Fig. 9(a) shows the morphology of the BFD raw material. The mineral particles are loosely distributed and vary substantially in size. The large particles have irregular surfaces with attached short rod-like fine particles, resulting in a porous structure. After ultrasound-assisted ammonia leaching (Fig. 9(c)) and ultrasound-activated $(NH_4)_2S_2O_8$ leaching (Fig. 9(e)), the large particles are fragmented into smaller irregular aggregates. Particle sizes in Figs. 9(a), 9(c), and 9(e) were measured using Nano Measurer 1.2 software (100 measurements for each sample), and the results are summarized in Table 2. The average particle sizes of the residues from ultrasound-assisted leaching and ultrasound-activated $(NH_4)_2S_2O_8$ leaching are 18.30 μm and 16.35 μm, respectively, both smaller than that of the raw material (23.26 μm). These observations suggest that the combined action of ultrasound and the leaching reagents promotes particle disruption, exposes more accessible reactive phases, and facilitates element leaching.

The EDS spectra in Fig. 9 qualitatively show that Fe, Zn, K, Na, and S are present in the raw material and residues. Compared with the raw material, the residues after ultrasound-assisted leaching and ultrasound-activated $(NH_4)_2S_2O_8$ leaching show markedly reduced local signals of Zn, K, Na, and S, while Fe remains relatively dominant. In particular, the lower local Zn and S signals in the persulfate-assisted residue are consistent with the leaching results and XRD analysis, suggesting enhanced removal of Zn-bearing phases, including ZnS.

3.3.3 Mechanism analysis

As shown in Fig. 10, the experimental observations obtained in this study, together with the findings reported in the literature, suggest a plausible mechanism for Zn leaching in the ultrasound-activated $(NH_4)_2S_2O_8$ system. Ultrasound is considered to promote particle fragmentation and interfacial renewal, thereby exposing fresh surfaces and improving contact between the leaching solution and the solid particles. This interpretation is supported indirectly by the reduced particle size and the fragmented morphology of the leaching residues. Meanwhile, persulfate can be activated under ultrasonic conditions to generate sulfate radicals ($SO_4^{\bullet-}$), which are likely responsible for the oxidation of refractory ZnS. Therefore, the enhanced Zn leaching is reasonably attributed to the combined effects of ultrasonic intensification and persulfate oxidation. However, this mechanistic interpretation is based on the experimental phenomena,

kinetic analysis, and literature reports, rather than on direct detection of cavitation behavior or sulfate radicals.

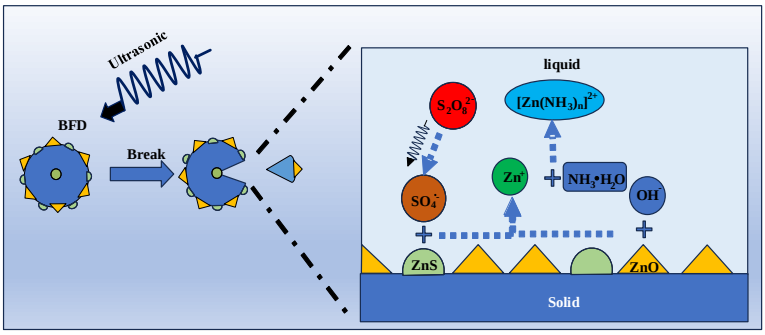

Fig. 10. Proposed mechanism of Zn leaching in the ultrasound-activated $(NH_4)_2S_2O_8$–$NH_3{\cdot}H_2O$–NH_4HCO_3 system.

4 Conclusions

In this study, the ultrasound-assisted $NH_3{\cdot}H_2O$–NH_4HCO_3 system was systematically investigated for the efficient recovery of valuable elements from blast furnace dust (BFD), and $(NH_4)_2S_2O_8$ was further introduced to enhance the leaching of refractory zinc-bearing phases. The main conclusions are as follows:

(1) Zn, K, and Na in BFD are efficiently co-leached by the ultrasound-assisted $NH_3{\cdot}H_2O$–NH_4HCO_3 system. Under the conditions of a total ammonia concentration of 6 $mol{\cdot}L^{-1}$, a solid-to-liquid ratio of 1:6, $[NH_3]/[NH_4^+]$= 1:1, a leaching temperature of 40 °C, and an ultrasonic power of 90 W, the leaching efficiencies of Zn, K, and Na reach 90.73%, 91.45%, and 91.56%, respectively, while Fe remains almost unleached, demonstrating excellent selectivity.

(2) Ultrasound-activated $(NH_4)_2S_2O_8$ further enhances the leaching of refractory zinc compounds. At an $(NH_4)_2S_2O_8$ concentration of 1.0 $mol{\cdot}L^{-1}$, a total ammonia concentration of 6 $mol{\cdot}L^{-1}$, a solid-to-liquid ratio of 1:6, $[NH_3]/[NH_4^+]$= 1:1, a leaching temperature of 40 °C, and an ultrasonic power of 90 W, the Zn leaching efficiency increases to 95.16%, which is 4.43% higher than that of ultrasound-assisted ammonia leaching and 11.51% higher than that of conventional ammonia leaching, while the leaching time is reduced by 16.67% and 66.67%, respectively. Meanwhile, the leaching efficiencies of K and Na slightly increased to 92.35% and 92.50%, respectively, while Fe leaching remained below 3%, confirming that the system maintained good selectivity after the addition of $(NH_4)_2S_2O_8$.

(3) The enhanced Zn leaching is reasonably attributed to the synergistic effects of ultrasonic intensification and persulfate oxidation, in which ultrasound promotes particle fragmentation, interfacial renewal, and mass transfer, while persulfate activation generates $SO_4^{\bullet-}$ radicals that facilitate the oxidation of refractory ZnS.

(4) Kinetic analysis indicated that Zn leaching in the $NH_3{\cdot}H_2O$–NH_4HCO_3 system was mainly controlled by the surface chemical reaction. The apparent activation energy decreased from 62.37 $kJ{\cdot}mol^{-1}$ under conventional leaching to 44.15 $kJ{\cdot}mol^{-1}$ under ultrasonic leaching, indicating that ultrasound reduced the energy barrier of Zn dissolution without changing the dominant rate-controlling step.

In this study, the simultaneous and efficient leaching of Zn, K, and Na from BFD

was achieved. Overall, the ultrasound-assisted $NH_3 \cdot H_2O$–NH_4HCO_3–$(NH_4)_2S_2O_8$ system provides an efficient and selective route for the recovery of Zn, K, and Na from BFD.

Data availability

The data in this study involves the core production technology and original operational data of the enterprise. Strict confidentiality obligations must be fulfilled, and the data cannot be disclosed to the public for the time being.

Conflict of interest

No potential conflict of interest was reported by the author(s).

References

[1] Li, Y., Feng, H., Wang, J., She, X., Wang, G., Zuo, H., Xue, Q. 2022. Current status of the technology for utilizing difficult-to-treat dust and sludge produced from the steel industry. J. Clean. Prod. 367, 132909. https://doi.org/10.1016/j.jclepro.2022.132909.

[2] Xinkai, H., Haitao, G., Yiming, S., Dan, W., Minsheng, L. 2020. Flotation and Dezincification on Blast Furnace Bag Dust and Application Analysis of Tailings. Non-Metallic Mines 43, 57–60. https://doi.org/10.3969/j.issn.1000-8098.2020.03.016.

[3] Moezzi, A., McDonagh, A. M., Cortie, M. B. Zinc oxide particles: Synthesis, properties and applications. Chemical Engineering Journal, 2012, 185–186: 1–22. https://doi.org/10.1016/j.cej.2012.01.076.

[4] Pan, H., Zhang, X., Wu, J., Zhang, Y., Lin, L., Yang, G., Deng, S., Li, L., Yu, X., Qi, H., Peng, H. 2016. Sustainability evaluation of a steel production system in China based on emergy. J. Clean. Prod. 112, 1498–1509. https://doi.org/10.1016/j.jclepro.2015.05.019.

[5] Ye F, Li M, Su S, et al. Separation and recovery of zinc from blast furnace dust via coordination leaching of Cl− and hydrolysis of NH4+[J]. Separation and Purification Technology, 2024, 330: 125361. https://doi.org/10.1016/j.seppur.2023.125361.

[6] Xue-feng, W.A.N., Dong, C.A.O., Xue-zhong, G.A.O., Shu-juan, Y.U., Xiao-lei, Z.H.U., Qing-tao, G.U.O. 2014. Technical research and practice of metallurgical dust recycling in converter. Sel. Pap. Eng. Chem. Metall. (China) 24, 35–41. https://doi.org/10.13228/j.boyuan.issn1006-9356.20140007.

[7] Zhang, D., Zhang, X., Yang, T., Rao, S., Hu, W., Liu, W., Chen, L. 2017. Selective leaching of zinc from blast furnace dust with mono-ligand and mixed-ligand complex leaching systems. Hydrometallurgy 169, 219–228. https://doi.org/10.1016/j.hydromet.2017.02.003.

[8] Mocellin, J., Mercier, G., Morel, J.L., Charbonnier, P., Blais, J.F., Simonnot, M.O. 2017. Recovery of zinc and manganese from pyrometallurgy sludge by hydrometallurgical processing. J. Clean. Prod. 168, 311–321. https://doi.org/10.1016/j.jclepro.2017.09.003.

[9] Asadi Zeydabadi, B., Mowla, D., Shariat, M.H., Fathi Kalajahi, J. 1997. Zinc recovery from blast furnace flue dust. Hydrometallurgy 47, 113–125. https://doi.org/10.1016/S0304-386X(97)00039-X.

[10] Boyanov, B., Peltekov, A., Petkova, V. 2014. Thermal behavior of zinc sulfide concentrates with different iron content at oxidative roasting. Thermochim. Acta 586, 9–16. https://doi.org/10.1016/j.tca.2014.04.005.

[11] Seyed Ghasemi, S.M., Azizi, A. 2018. Alkaline leaching of lead and zinc by sodium hydroxide: kinetics modeling. J. Mater. Res. Technol. 7, 118–125. https://doi.org/10.1016/j.jmrt.2017.03.005.
[12] Ma A, Li J, Chang J, et al. Mechanism analysis and experimental research on leaching Zn from zinc oxide dust with an ultrasound-enhanced NH3-NH4Cl-H2O system[J]. Sustainability, 2024, 16(7): 2901.
[13] Yang S, Zhao D, Jie Y, et al. Hydrometallurgical process for zinc recovery from CZO generated by the steelmaking industry with ammonia–ammonium chloride solution[J]. Metals, 2019, 9(1): 83. https://doi.org/10.3390/met9010083.
[14] Jia, L., Zhong, Y., Li, K., Li, B., Gao, J., Liu, T., Wang, F., Wu, W., Feng, J. 2023. Recovery of zinc resources from secondary zinc oxide via composite ammonia leaching: Analysis of Zn leaching behavior. Chem. Eng. J. 472, 144930. https://doi.org/10.1016/j.cej.2023.144930.
[15] Rodriguez Rodriguez, N., Gijsemans, L., Bussé, J., Roosen, J. Önal, M.A.R., Masaguer Torres, V., Manjón Fernández, Á., Jones, P.T., Binnemans, K., 2020. Selective Removal of Zinc from BOF Sludge by Leaching with Mixtures of Ammonia and Ammonium Carbonate. J. Sustain. Met. 6, 680–690. https://doi.org/10.1007/s40831-020-00305-3.
[16] Xing-guo, L.U.O., Chang, W.E.I., Xing-bin, L.I. 2019. Removal of zinc from blast furnace dust by ammonia-ammonium carbonate. Chin. J. Nonferrous Met. 29, 2433–2441. https://doi.org/10.19476/j.ysxb.1004.0609.2019.10.24.
[17] Li, H., Zhao, L., Wang, L., Liang, J., Yan, H., Liu, J. 2021. Leaching Kinetics of Secondary Zinc Oxide in a NH3–NH4HCO3–H2O System. Crystals (Basel) 11, 496. https://doi.org/10.3390/cryst11050496.
[18] Liu, J., Wang, S., Zhang, Y., Zhang, L., Kong, D. 2022. Synergistic mechanism and decopperization kinetics for copper anode slime via an integrated ultrasound-sodium persulfate process. Appl. Surf. Sci. 589, 153032. https://doi.org/10.1016/j.apsusc.2022.153032.
[19] Yang, S., Yang, H., Wang, F., Song, X., Cui, S., Feng, J., Ning, P., Jia, L. 2025. Efficient recovery of zinc resources from high chloride zinc slag via ammonia-ammonium sulfate-ammonium persulfate system. Sep. Purif. Technol. 362, 131765. https://doi.org/10.1016/j.seppur.2025.131765.
[20] Gui, Q., Fu, L., Hu, Y., Di, H., Liang, M., Wang, S., Zhang, L., Dong, E. 2023. Oxidative pretreatment of refractory gold ore using persulfate under ultrasound for efficient leaching of gold by a novel eco-friendly lixiviant: Demonstration of the effect of particle size and economic benefits. Hydrometallurgy 221, 106110. https://doi.org/10.1016/j.hydromet.2023.106110.
[21] Suslick, K.S., Hyeon, T., Fang, M., Cichowlas, A.A. 1995. Sonochemical synthesis of nanostructured catalysts. Mater. Sci. Eng. A Struct. Mater. 204, 186–192. https://doi.org/10.1016/0921-5093(95)09958-1.
[22] Dang, Y., Yang, Z., Lin, G., Zhai, B., Zhang, H., Sheng, X., Li, S., Zhang, L. 2025. Mechanism of leaching zinc from low-grade zinc oxide by ultrasonic enhancement. Chem. Eng. Process. 209, 110203. https://doi.org/10.1016/j.cep.2025.110203.

[23] Kanthale, P., Ashokkumar, M., Grieser, F. 2008. Sonoluminescence, sonochemistry (H2O2 yield) and bubble dynamics: Frequency and power effects. Ultrason. Sonochem. 15, 143–150. https://doi.org/10.1016/j.ultsonch.2007.03.003.
[24] Skorina T, Allanore A. Aqueous alteration of potassium-bearing aluminosilicate minerals: from mechanism to processing[J]. Green Chemistry, 2015, 17(4): 2123-2136.
[25] Aydogan S, Aras A, Canbazoglu M. Dissolution kinetics of sphalerite in acidic ferric chloride leaching[J]. Chemical Engineering Journal, 2005, 114(1-3): 67-72. https://doi.org/ 10.1016/j.cej.2005.09.005.
[26] Pinho, S.C., Ribeiro, C., Ferraz, C.A., Almeida, M.F. 2021. Copper, zinc, and nickel recovery from printed circuit boards using an ammonia–ammonium sulphate system. J. Mater. Cycles Waste Manag. 23, 1456–1465. https://doi.org/10.1007/s10163-021-01226-3.
[27] Zhang Y-M, Li J, Chen Q-Y, et al. Influence of ultrasonic irradiation on ammonia leaching of zinc from low-grade oxide zinc ore [J]. The Chinese Journal of Nonferrous Metals, 2009, 19(05): 960-6. https://doi.org/10.3321/j.issn:1004-0609.2009.05.028.
[28] Qi, Y., Chen, J., Xu, H., Wu, S., Yang, Z., Zhou, A., Hao, Y. 2024. Optimizing sludge dewatering efficiency with ultrasonic Treatment: Insights into Parameters, Effects, and microstructural changes. Ultrason. Sonochem. 102, 106736. https://doi.org/10.1016/j.ultsonch.2023.106736.
[29] Bu, X., Danstan, J.K., Hassanzadeh, A. Behrad Vakylabad, A., Chelgani, S.C., 2024. Metal extraction from ores and waste materials by ultrasound-assisted leaching -an overview. Miner. Process. Extr. Met. Rev. 45, 28–45. https://doi.org/10.1080/08827508.2022.2117173.
[30] Chen, X., Wang, J., Guo, Y., Zeng, H., Xuan, K., Guo, Y., Jiang, H., Wang, X., Zhou, Z. 2023. Enhanced reduction of uranium (VI) in groundwater via regulation of heat-activated persulfate: The role of formate and its mechanisms. J. Environ. Chem. Eng. 11, 110299. https://doi.org/10.1016/j.jece.2023.110299.
[31] Xu, Y., Xia, H., Zhang, Q., Cai, W., Jiang, G., Zhang, L. 2022. Green and efficient recovery of valuable metals from by-products of zinc hydrometallurgy and reducing toxicity. J. Clean. Prod. 380, 134993. https://doi.org/10.1016/j.jclepro.2022.134993.
[32] Jiang, H., Wang, J., Zhou, A., Liu, Y. 2024. Rapid Oxidation of Ammonia Nitrogen to Nitrogen Gas by UV-Activated Persulfate with Calcium Oxide. ACS ES T Eng. 4, 1092–1101. https://doi.org/10.1021/acsestengg.3c00566.
[33] Wang, H.H., Li, G.Q., Zhao, D., Ma, J.H., Yang, J., 2017. Dephosphorization of high phosphorus oolitic hematite by acid leaching and the leaching kinetics. Hydrometallurgy 171, 61–68. https://doi.org/10.1016/j.hydromet.2017.04.015.